Alginate Operates as a Dual Inhibitor of Barite Nucleation and Crystal Growth

Journal:	*Molecular Systems Design & Engineering*
Manuscript ID	ME-ART-02-2021-000010.R1
Article Type:	Paper
Date Submitted by the Author:	07-Apr-2021
Complete List of Authors:	Geng, Xi; University of Houston, Chemical Engineering Sosa, Ricardo; University of Houston, Reynolds, Michael; Shell Upstream Americas, Completions & Technology Effectiveness team Conrad, Jacinta; University of Houston, Rimer, Jeffrey; University of Houston, Chemical and Biomolecular Engineering

Design, System, Application

A method of inhibiting the formation of inorganic scale was designed wherein alginate, a bio-derived acidic polysaccharide from brown algae, is explored as an alternative to commercial scale treatments. The system examined in this study is barium sulfate (barite), which is a common scale that poses systemic problems owing to its low solubility. Our findings reveal that alginate is unique based on its ability to fully suppress both nucleation and crystal growth. The impact of alginate on barite crystallization was studied at a macroscopic level using time-resolved microfluidics experiments to reveal alginate's affinity to interact with all principal crystallographic faces of barite, which is uncommon among inhibitors reported in literature. The mechanism of growth inhibition was explored at a near molecular level using *in situ* atomic force microscopy to probe the interactions between alginate and barite crystal surfaces. The immediate application of alginate-based treatment involves the remediation of mineral scale, which is an undesirable and ubiquitous phenomenon in industrial systems for wastewater treatment, energy production, and manufacturing. The findings in this study highlight the dual roles and exceptional performance of alginate as a promising and green alternative to current barite scale treatments.

Alginate as a Green Inhibitor of Barite Nucleation and Crystal Growth

Xi Geng,[1‡] Ricardo D. Sosa,[1‡] Michael A. Reynolds[2]*, Jacinta C. Conrad[1]*, Jeffrey D. Rimer[1]*

[1] Department of Chemical and Biomolecular Engineering, University of Houston, Houston, Texas 77204, United States

[2] Shell Exploration and Production Company, Houston, TX 77079, USA

* Correspondence sent to:
Mike.Reynolds@shell.com, jcconrad@uh.edu, and jrimer@central.uh.edu

‡ These authors contributed equally to this work

Abstract

Few (macro)molecular inhibitors of inorganic scale can suppress both nucleation and crystal growth. In this study, we examine a series of potential inhibitors of barium sulfate (barite), which is a common scale that poses systemic problems owing to its low solubility. We show that alginate (an acidic polysaccharide) is an anomaly among a diverse set of carboxylate-based modifiers of barite crystallization based on its ability to completely suppress both nucleation and crystal growth. Bulk crystallization assays reveal that alginate completely suppresses barite nucleation. Experiments to quantify barite crystal growth kinetics at the macroscopic level under different flow conditions revealed that alginate is also a potent inhibitor of crystal growth, with full suppression of crystallization occurring at modifier concentration of 60 nM. Time-resolved microfluidics experiments revealed alginate's affinity to interact with all principal crystallographic faces of barite, which is uncommon among inhibitors of various inorganic crystals reported in literature. *In situ* atomic force microscopy experiments to probe the interactions between alginate and barite crystal surfaces revealed a transition from step bunching to step pinning modes of action at low and high alginate concentrations, respectively. The findings in this study highlight the dual roles and exceptional performance of alginate as a barite scale inhibitor. Owing to its natural abundance in brown algae, alginate is a promising and green alternative to current scale treatments.

Introduction

Mineralization of alkaline earth metals and iron-based scale components is an undesirable and ubiquitous phenomenon in industrial systems for wastewater treatment, energy production, and manufacturing.[1-3] One of the most stubborn components of mineral scale is barium sulfate (i.e. barite).[4,5] Approaches to prevent barite scale include treatments with phosphonate-based commercial inhibitors such as diethylenetriamine penta(methylene phosphonic acid) (DETPMP), hydroxyethylidene diphosphonic acid (HEDP), or related analogues.[1, 4, 6-10] Carboxylate-based compounds are generally less potent, and thus have received less attention as commercial scale inhibitors, but are frequently employed as chelating agents of alkaline earth metals (e.g. Ba^{2+} and Ca^{2+}). Examples include ethylenediaminetetraacetic acid (EDTA) and diethylene-triaminepentaacetic acid (DTPA) owing to their strong binding affinity for metal ions.[11-15] Most commercial compounds used to treat barite scale are not easily biodegradable. Moreover, one drawback of carboxylate-based compounds is the required use of caustic (highly alkaline) solutions to dissociate acid groups for improved efficacy.[16, 17] Thus, there remains a need for environmentally friendly alternatives to effectively inhibit mineral scale.

Inspiration for the design of novel crystal growth inhibitors can be drawn from natural compounds (or their derivatives) that regulate biomineralization.[18-23] One class of natural carboxylate-based compounds with broad appeal are polysaccharides owing to their ability to regulate the crystallization of numerous minerals. These species are generally referred to as modifiers, but more specifically they are denoted as either promoters or inhibitors of crystallization. Polygalacturonic acid is a bioinspired compound reported to inhibit barite crystallization.[24] Additional examples include carboxymethylcellulose (CMC) and carboxymethyl inulin,[25-27] which are effective inhibitors of calcium oxalate and calcium carbonate. One

polysaccharide that has shown promise is alginate, a linear biopolymer constructed from mannuronic acid (M) and guluronic acid (G) monomers, which is extracted from brown sea algae and is used commercially as an additive in consumer goods.[28-30] Although its efficacy has not been tested previously for barite, it has been demonstrated that alginate is an effective inhibitor of calcium and magnesium based scales[31] and crystals such as calcite ($CaCO_3$), hydroxyapatite ($Ca_{10}(PO_4)_6(OH)_2$), and struvite ($NH_4MgPO_4 \cdot 6H_2O$), and a mild inhibitor of brushite ($CaHPO_4 \cdot 2H_2O$) crystallization.[32-39]

The efficacy of an inhibitor is determined by its ability to suppress nucleation and/or crystal growth. It is less common to encounter compounds capable of fully suppressing nucleation, and also unusual to find a compound with dual capability to inhibit both nucleation and growth. There are a few phosphonate-based compounds that inhibit barite nucleation (e.g. HEDP and phosphinopolycarboxylic acid, PPPC).[40-42] To our knowledge there are no examples of barite nucleation inhibitors containing only carboxylate moieties; prior studies have instead reported exclusively on the efficacy of carboxylate-based compounds as inhibitors of crystal growth.[11, 13-15, 23, 24, 41, 43] Barite grows via a classical layer-by-layer process involving the addition of monomer (solute) from solution to crystal surface sites (i.e. kinks, steps, and terraces).[44] Growth inhibitors for a variety of systems reduce the rate of solute addition to crystal surfaces by two predominant mechanisms: kink blocking and step pinning.[45] Kinks are the most favorable sites for solute incorporation; thus, the adsorption of inhibitors to these sites can dramatically reduce (but not fully impede) the rate of step advancement.[46, 47] A more effective mechanism of growth inhibition is step pinning wherein modifiers adsorb on terraces and suppress step growth by imposing a surface tension on advancing layers.[47, 48] A common attribute of crystal growth inhibitors is their preference for binding to select crystallographic surfaces, which alters the anisotropic kinetics of

growth.[45, 49] This binding specificity enables certain facets to grow at the expense of others that are either fully or partially inhibited, which can explain why there are few inhibitors that are capable of fully suppressing crystallization.

Hydrodynamics can play an important role in scale treatment. It has been demonstrated that higher rates of fluid flow minimize barriers for inhibitor diffusion to barite surfaces, thereby improving modifier efficacy.[50-52] Turbulent rotary flow[53] in the presence of modifiers has been shown to enhance crystal growth inhibition, whereas stirring[50] can reduce an inhibitor's efficacy relative to quiescent conditions. The effects of laminar fluid flow conditions on crystal growth inhibition can be probed at different length scales.[4] Microfluidics offers a unique platform to investigate bulk crystallization kinetics and time-resolved morphological development of crystals at the macroscopic level,[51, 52] whereas *in situ* atomic force microscopy (AFM) can be used to extract mechanistic details of surface growth inhibition at near molecular level.[45, 54-57]

In this study, we use a combination of microfluidics, AFM, and other techniques to assess a series of polycarboxylates as potential barite scale inhibitors under quiescent and flow conditions. Bulk assays reveal a wide disparity in efficacy of polycarboxylates as inhibitors of barite crystallization. Among the compounds investigated, we identified two macromolecules – alginate and polygalacturonic acid – that are capable of inhibiting barite nucleation. Microfluidic assays revealed that alginate was also a potent inhibitor of barite crystal growth, showing that alginate fully suppresses barite crystallization. Furthermore, *in situ* AFM studies reveal two distinct mechanisms of layer growth inhibition on barite crystal surfaces that are dependent upon the concentration of alginate. Based on these findings, alginate emerges as a sustainable alternative to commercial additives owing to its dual role as a nucleation and growth inhibitor.

Experimental Methods

Materials. The following reagents were purchased from Sigma Aldrich: barium chloride dihydrate (99+%), sodium sulfate (>99%), sodium hydroxide (>97%), and sodium chloride (>99.5%), sodium citrate tribasic dihydrate (≥99.0%), sodium alginate from algae brown, succinic acid, tricarballylic acid, 1,2,3,4-butanetetracarboxylic acid, ethylenediaminetetraacetic acid (EDTA), and diethylenetriaminepentaacetic acid (DTPA). Sodium alginate (Grindsted FD 120) was provided by Danisco. Polydimethylsiloxane (PDMS, Dow Corning SYLGARD 184) was purchased from Essex Brownell, and SU-8 2150 photoresist and SU-8 developer were purchased from Microchem. All chemicals were used as received without further purification. Silicone tubing was purchased from Cole-Parmer. Single-side polished 4-inch P-type silicon wafers <100> were purchased from University Wafer and were cleaned using a piranha solution. Deionized (DI) water used in all experiments was filtered with an Aqua Solutions RODI-C-12A purification system (18.2 MΩ·cm).

Bulk crystallization assays. Barite crystals were synthesized using a protocol modified from procedures reported in the literature.[7, 58-62] In a typical synthesis, $NaCl_{(aq)}$ was first added into a 20-mL glass vial followed by aliquot addition of 10 mM $BaCl_{2,(aq)}$ and 10 mM $Na_2SO_{4,(aq)}$ stock solutions under mild agitation for 10 s. Samples prepared in the presence of molecular modifiers were carried out by adding aliquots of molecular modifiers $_{(aq)}$ to the reaction mixture prior to the addition of Na_2SO_4. The final growth solutions with a total volume of 10 mL had a pH of 7.1 ± 0.3 and a composition of 0.5 mM $BaCl_2$: 0.5 mM Na_2SO_4 : 600 mM NaCl : x μg mL^{-1} modifier ($0 \leq x \leq 10$). The sample vials were left undisturbed at 22 °C for 24 h to allow crystallization of hexagonal barite platelets with well-defined (001), (210), and (100) facets.

Microfluidic assays in the presence of inhibitors. To quantify the inhibition efficacy, the seeded growth of barite crystals was imaged over time using an inverted optical microscope. Microfluidic devices were assembled (Figure S1) and seeded with barite crystals using a previously reported method.[52] Two solutions were prepared and transferred into separate syringes. One solution contained 0.5 mM $BaCl_2$ and the second solution contained 0.5 mM Na_2SO_4, 1.2 M NaCl and various quantities of growth modifiers (0 – 20 μg mL^{-1}). The two solutions were mixed using an inline flow configuration that produced a final composition of 0.35 mM $BaCl_2$, 0.35 mM Na_2SO_4, 600 mM NaCl and inhibitors at varied concentration. The fully mixed growth solution was introduced into seeded PDMS chips using a dual syringe pump where inhibitors were added to the syringe containing SO_4^{2-} to minimize formation of ion complexes. Growth solutions were mixed through silicon tubing attached to a y-connector, and then successively fed into the corresponding inlet of the concentration gradient generator.

Materials characterization and Instrumentation. Powder X-ray diffraction (PXRD) patterns of natural and as-synthesized samples were collected on a Rigaku Smart Lab X-ray diffractometer using a Cu-Kα radiation source (λ = 1.5406 Å, 40 kV, 30 mA). Reference PXRD patterns were selected from the ICDD PDF-2 2013 database.[63] Dual star benchtop pH/ISE meters (Orion) equipped with a ROSS Ultra electrode (8102BNUWP) was used for adjusting pH with 10 mM solutions of NaOH and HCl. Conductivity measurements were carried out to assess the crystallization kinetics in the presence of crystal modifiers. Conductivity probe (VWR, 515 conductivity dip cell coated with Au) was vertically immersed into the growth solution under magnetic stirring (600 rpm) and the readings were recorded by the conductivity meter (VWR EC meter, model 2052). The conductivity probe was calibrated with 0.005 M KCl standard solutions prior to the experiments.

For *ex situ* microscopy measurements, a clean glass slide (1 cm^2) was positioned at the bottom of the vials to collect barite crystals. After crystallization, the glass slide was removed from its solution, gently rinsed with de-ionized (DI) water, and dried in air prior to analysis. SEM samples were prepared by attaching carbon tape to SEM studs and subsequently attaching glass slides to carbon tape by gently pressing the glass slide to the tape using tweezers. Scanning electron microscope (SEM) images were obtained on a FEI 235 dual-beam (focused ion-beam) system operated at an accelerating voltage of 15 kV and a working distance of 5 mm. As-synthesized samples were prepared by gently pressing the glass slide containing crystals onto the carbon tape. All the samples were coated with a thin layer of gold (ca. 5 – 10 nm) prior to imaging.

The size and morphology of barite crystals were examined using Leica DM2500-M optical microscope in transmittance mode, and *in situ* imaging of crystal growth was performed on the Leica DMi8 inverted optical microscope using transmittance mode equipped with HC PL Fluotar 5×, 10×, 20×, and N Plan L 50× objectives. To characterize crystals grown in the quiescent bulk assay, at least ten brightfield images of representative areas on the bottom of the glass vials were captured in transmittance mode. The average [010] length, [100] width, and [001] thickness of crystals in optical micrographs were measured from a minimum of 100 crystals per trial and three separate trials. *In situ* time-resolved studies were evaluated using a Leica DMi8 inverted optical microscope equipped with a motorized stage and LAS X software. Images were captured in transmittance mode along a minimum of 20 positions throughout a seeded microchannel at 10 – 30 min intervals for at least 3 h. Crystals observed *in situ* were analyzed using ImageJ (NIH) and the detailed analytical protocol is described in our previous work.[52] From the change in crystal length over time, a growth rate r was determined for each experimental condition. The relative length ratio (RLR) and relative growth rate (RGR) were calculated as

$$RLR = \frac{L_m}{L_c} \quad (1)$$

$$RGR = \frac{r_m}{r_c} \quad (2)$$

where L_m and L_c represent the length of crystals grown in the presence of a modifier (m) and in the absence of any additive (c, control). The parameters r_m and r_c represent growth rates in the presence and absence of a growth modifier, respectively.

Atomic force microscopy. In situ atomic force microscopy (AFM) was performed to examine the temporal changes in topographical features on barite crystal surfaces. Barite crystals prepared via the bulk crystallization method described previously were synthesized directly onto an AFM specimen disk (Ted Pella) covered with a thin layer of thermally curable epoxy (Loctite, China). The epoxy was first partially cured in an oven for ca. 5 min at 60 °C prior to drying in air overnight to completely cure the epoxy. The AFM specimen disks were placed at the bottom of 20 mL glass vials and reagents used for bulk crystallization of barite were subsequently introduced to the vials upon which crystals nucleated, sedimented onto the epoxy, and grew overnight. The samples were then rinsed in DI water and exposed to a growth solution (supersaturation ratio of S = 4.4) containing only Ba^{2+} and SO_4^{2-} ions for 1 hour prior to imaging. All AFM measurements were performed in a Cypher ES instrument (Asylum Research, Santa Barbara, CA) using silicon nitride probes with fold reflex coating and a spring constant of 0.15 N/m (Olympus, TR800PSA). The liquid cell (ES-CELL-GAS) contained two ports for inlet and outlet flow to maintain constant supersaturation during AFM measurements. Growth solutions containing different concentrations of solute ($BaCl_2$, Na_2SO_4) and inhibitors were delivered to the liquid cell using a y-connector mixing configuration where both solute solutions were combined immediately before entering the cell (analogous to the microfluidics configuration). Continuous imaging was performed at ambient temperature in contact mode with a scan rate of 2.44 Hz at 256 lines per scan.

Results and Discussion

Identifying Potent Inhibitors of Barite Crystallization

We selected nine different polyprotic acids (Figure 1, molecules labelled by I – IX) as potential inhibitors of barite crystallization. These molecules include polycarboxylic acids (I – IV), aminopolycarboxylic acids (V and VI), and biomacromolecules such as alginate (VIII) that is composed of two different monomers, D-glucuronic acid (VII) and mannuronic acid, and lastly polygalacturonic acid (IX), which has a ring structure and chemical functionality similar to both monomers of alginate. The library of modifiers was screened in bulk crystallization assays under quiescent conditions to evaluate their efficacy *ex situ*, as determined from changes in the size, morphology, and number density of crystal populations. Growth solutions used for these bulk assays were prepared with a supersaturation ratio of S = 10 (pK_{sp} of barite = 9.97 at 25 °C).[64]

Barite crystals obtained from bulk assays in the absence of a modifier (control) exhibit a hexagonal coffin-shaped morphology (Figure 2a,e). At low modifier concentration (1 μg mL^{-1}), we observed no apparent change in barite crystal morphology (Figure S2) when using the following molecules: succinic acid, tricarballylic acid, tetracarboxylic acid, and D-guluronic acid. Conversely, the addition of 1 μg mL^{-1} of citrate (Figure 2b,f), EDTA (Figure S2), or DTPA (Figure 2c,g) had a pronounced impact on barite morphology. The latter two directed the formation of barite crystals with irregular features, whereas citrate preferentially binds to the apical tips of barite crystals to elongate them along the a-direction (Figure S2). Except for citrate, molecules containing fewer than 4 carboxylates had a moderate effect on barite crystal morphology. Interestingly, there were almost no crystals detected in bulk assays with 1 μg mL^{-1} of alginate (Figure 2d) in the standard timeframe of measurement (ca. 24 h) as well as extended analysis over a 10 day period.

Trace particles with a globular, unidentifiable morphology (Figures 2h and S3) were observed at a lower alginate concentration.

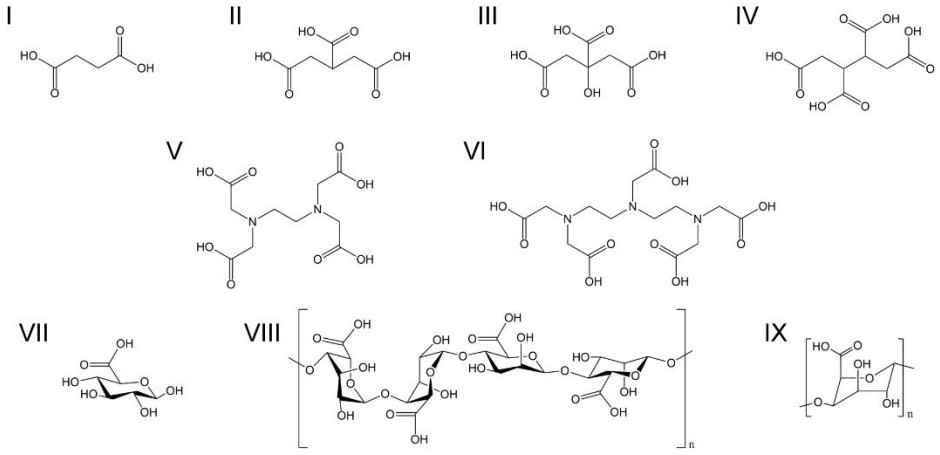

Figure 1. Chemical structures of molecules tested as putative growth modifiers of barite crystallization: (I) succinic acid; (II) tricarballylic acid; (III) citric acid; (IV) 1,2,3,4-butanetetracarboxylic acid; (V) ethylenediaminetetraacetic acid (EDTA); (VI) diethylenetriamine pentaacetate (DTPA); (VII) D-glucuronic acid; (VIII) alginic acid (or alginate); and (IX) polygalacturonic acid (PA). Note that mannuronic acid was not included in the list due to availability constraints.

A ten-fold increase in a given modifier concentration (10 μg mL^{-1}) resulted in more pronounced changes to barite crystal morphology (Figure S4), apart from succinic acid, tricarballylic acid, and D-guluronic acid. Growth solutions containing 10 μg mL^{-1} of citrate produced crystals with spheroidal features. Tetracarboxylic acid produced crystals with shapes similar to those observed with EDTA at lower concentration (Figure S2), whereas EDTA at higher concentration resulted in thin, needle-like crystals that were often observed to form aggregates in a spherulitic conformation (Figure S4). Bulk assays in the presence of DTPA generated crystals with round edges (i.e. lack of distinct facets). Similarly, assays with 10 μg mL^{-1} polygalacturonic acid resulted in aggregates of spherical crystals, similar to those in the presence of alginate at much lower concentrations (Figure S3). Powder XRD patterns of all crystals confirmed the formation of crystalline barium

sulfate (Figure S5); however, crystals synthesized in the presence of macromolecules resulted in yields (ca. μg per batch) too low to determine crystallinity via powder XRD.

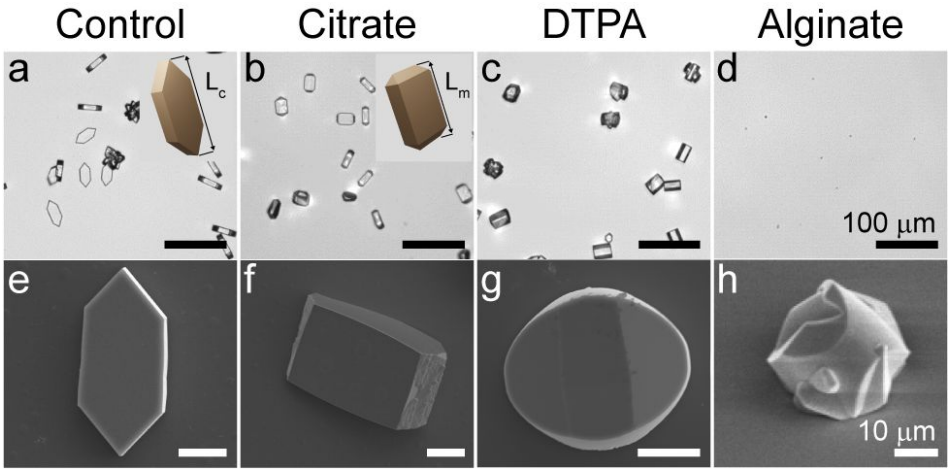

Figure 2. Optical (a – d) and scanning electron (e – h) micrographs of barite crystals synthesized under quiescent conditions at S=10 in the absence of modifiers (a and e) and in the presence of (b and f) 1 μg mL^{-1} citrate, (c and g) 1 μg mL^{-1} DTPA, (d) 1 μg mL^{-1} alginate, and (h) 0.5 μg mL^{-1} alginate. Scale bars equal 100 μm and 10 μm for the top and bottom rows, respectively. Insets: crystal habit with L_c and L_m labelled as the average length of barite in the absence or presence of inhibitors, respectively.

Crystal growth inhibition resulting from specific interactions between modifiers and crystal surfaces can be gleaned from changes in relative crystal dimensions (e.g. the length measured along the fastest growth direction, [010]). The effect of modifiers on crystal habit were grouped into one of two general categories, (i) well-defined morphologies and (ii) irregular particles, and quantified with respect to the control (i.e. no modifier) using a relative length ratio (RLR, Eq. 1). At the highest modifier concentration tested (10 μg mL^{-1}), only a subset of molecules resulted in more than 50% reduction in barite crystal length. These include citrate (III), tetracarboxylate (IV), EDTA (V), DTPA (VI), and alginate (VIII) (Figure 3a). The latter three stand out as exemplary inhibitors (i.e. >80% reduction in RLR). At the lowest modifier concentration tested (1 μg mL^{-1}), the impact of alginate on RLR is almost unchanged whereas the other molecules are far less effective (Figure 3b).

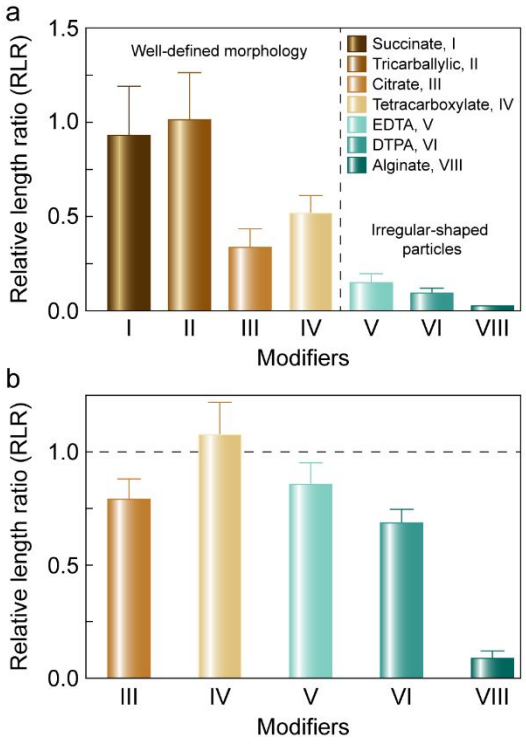

Figure 3. Histograms comparing the efficacy of modifiers based on their alteration of the relative length ratio (RLR), as defined in Eq. 1, at two different modifier concentrations: (a) 10 μg mL^{-1} and (b) 1 μg mL^{-1}. Bulk crystallization assays were performed in growth solutions of constant supersaturation (S = 10) under quiescent conditions. Average measurements of crystal dimensions from optical micrographs are reported for 3 separate trials with more than 100 measurements per trial. Error bars equal one standard deviation. The vertical dashed line separates modifiers leading to well-defined (left) and irregular (right) barite crystal morphologies whereas the horizontal dashed line indicates no change in length relative to the control.

Table 1. Number density of barite crystals in bulk crystallization assays.[a]

Polycarboxylate	Sample	Number density (mm^{-2}) [b]	
		1 μg mL^{-1}	10 μg mL^{-1}
Succinic acid	I	7.9 ± 0.4	4.8 ± 0.3
Tricarballylic acid	II	9 ± 1	11 ± 1
Citrate	III	7.1 ± 0.6	16 ± 1
Tetracarboxylic acid	IV	8.5 ± 0.4	4.9 ± 0.3
EDTA	V	4.0 ± 0.5	3.9 ± 0.2
DTPA	VI	13 ± 1	38 ± 2
D-Guluronic acid	VII	9.2 ± 0.7	3.0 ± 0.5
Polygalacturonic acid	IX	2.5 ± 0.1	1.0 ± 0.1
Alginate	VIII	0	0

a. measurements in supersaturated solutions (S = 10) under quiescent conditions; b. number density of the control is 5.2 ± 0.7 mm^{-2}

Impact of Inhibitors on Barite Nucleation

The effect of modifiers on barite nucleation was inferred by measuring changes in the number density of barite crystals as an indicator of a modifier's mode of action. Promotion of nucleation generally results in a larger population of crystals, whereas inhibition of nucleation yields fewer crystals. To assess the impact of each modifier, the average number density of crystals after bulk crystallization assays (Table 1) was compared against a control sample (5.2 ± 0.7 crystals mm^{-2}) synthesized at the same supersaturation (S = 10) in the absence of any modifier. Within the error of measurement, most modifiers had negligible effect on nucleation. At the highest modifier concentration tested, three compounds appear to promote nucleation. DTPA (VI) produced the highest number density of crystals (nearly 8-fold higher than the control), and citrate (III) and tricarballylic acid (II) resulted in 4- and 2-fold increases, respectively. Conversely, both macromolecules (polygalacturonic acid (IX) and alginate (VIII)) were the only modifiers that inhibit nucleation. Notably, alginate is unique among the modifiers tested based on its ability to prevent nucleation at both low and high concentration. To our knowledge, this is the first evidence that a single modifier is capable of fully suppressing barite nucleation at environmentally friendly conditions (pH = 7) without the use of Ba^{2+} sequestering agents.

Impact of Inhibitors on the Kinetics of Barite Crystallization

The kinetics of barite crystallization were evaluated by tracking the temporal depletion of Ba^{2+} and SO_4^{2-} ions from a supersaturated barite growth solution in the absence and presence of each modifier using ionic conductivity. Unlike the previous bulk crystallization assays, these studies were conducted under stirring (at 400 rpm) to reduce the induction period and overall time of crystallization. These measurements cannot fully decouple the effects of nucleation from crystal growth, but do allow for direct assessment of modifier efficacy. We determined the rate of

crystallization from the initial (approximately linear) decrease in conductivity with time from de-supersaturation curves (Figure S6), and report the relative growth rate (RGR, Eq. 2) using as a reference the value obtained from a supersaturated growth solution (control) in the absence of modifier (Figure 4). A value of RGR = 1 signifies no change in the rate of growth, whereas RGR < 1 indicates crystal growth inhibition.

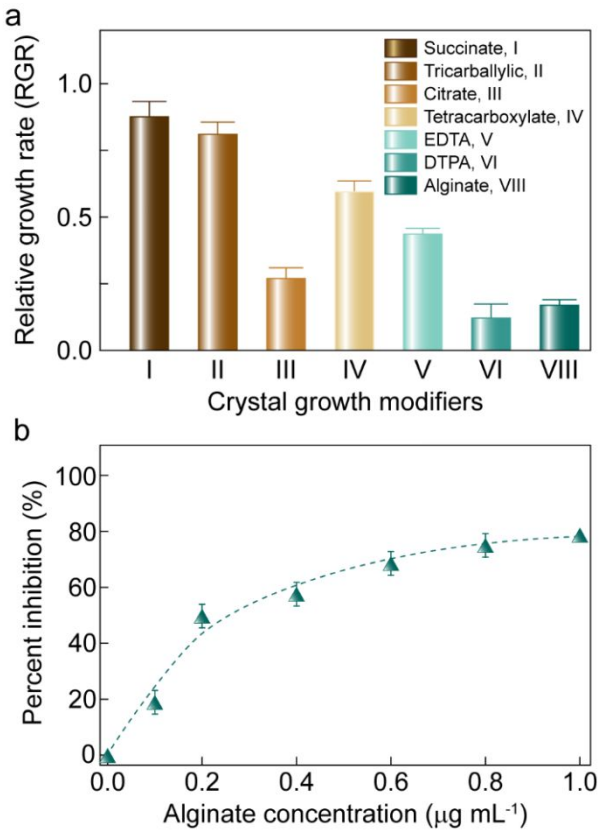

Figure 4. (a) Relative growth rate (RGR) determined from the linear slope of de-supersaturation curves (Figure S6) measured under constant stirring in growth solutions (S = 10) containing 1 μg mL^{-1} of each modifier. Histograms are the average of at least three separate experiments. Error bars equal one standard deviation. (b) Percent inhibition of barite growth as a function of alginate concentration. Corresponding de-supersaturation curves are provided in Figure S7. Percent inhibition was calculated as (1-RGR) × 100%. Symbols are the average from at least three separate experiments. Error bars span two standard deviations and the dashed line is interpolated to guide the eye.

The modifiers can be grouped in general categories based on their relative efficacy: weak inhibitors (I and II), moderate inhibitors with RGR $\approx$ 0.5 (IV and V), and strong inhibitors with

RGR < 0.25 (III, VI, and VIII). These results contrast with those from the bulk assays under quiescent conditions (Figure 3b), in which alginate (VIII) significantly outperforms all other modifiers. This comparison indicates that agitation (or stirring) reduces alginate's efficacy, leading to a maximum 80% inhibition of barite crystallization (Figure 4b) compared to the complete suppression of nucleation observed under quiescent conditions (Table 1). These results are analogous to other mineral systems, such as struvite, in which a transition from stirring to quiescent conditions enhances the efficacy of crystal growth inhibitors.[50]

Effect of Potent Inhibitors on Anisotropic Crystal Growth

To evaluate the effects of alginate on the anisotropic rates of barite crystallization, we used a microfluidic platform to track temporal changes in the macroscopic dimensions of crystals under controlled flow rates (i.e. fixed Reynolds number Re = 9.2). Benefits of using microfluidics include the ability to (i) maintain a constant supersaturation, (ii) decouple the effect of modifiers on crystal growth relative to nucleation, and (iii) quantify the anisotropic rates of growth for all relevant crystal facets at a macroscopic level. For these studies we prepared seeded microfluidic devices and slightly reduced the supersaturation of the growth medium (S = 7.0) to prevent the formation of new nuclei. Seed crystals in the microchannels that were exposed to growth solutions without inhibitors grew anisotropically with a fixed aspect ratio. To account for alginate inhibition of growth, we monitored the basal (001) surface and tracked temporal changes in the length and width of crystals along the b- and a-directions, respectively. The growth rates in the presence of each additive (Figure 5) were compared against the control to calculate relative growth rates (RGR) for alginate as well as two additional compounds, DTPA and citrate, which were identified as strong inhibitors (Figure 4a).

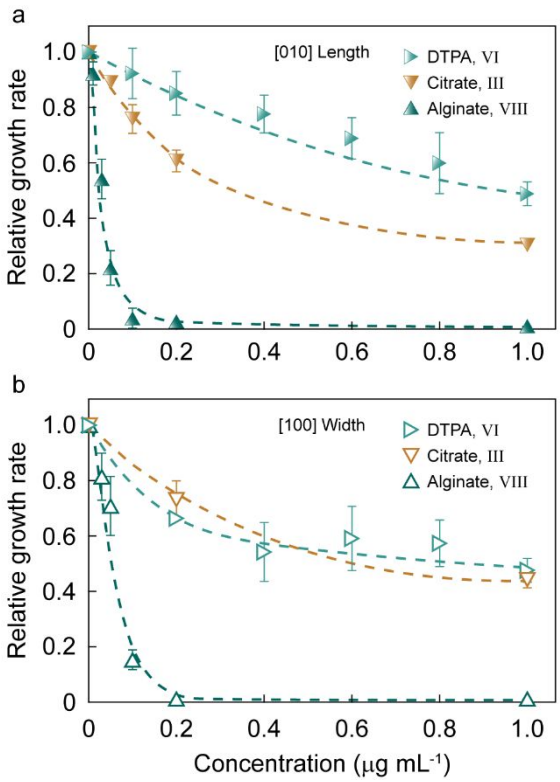

Figure 5. Relative growth rate (RGR) of barite crystallization based on (a) crystal width and (b) crystal length dimensions as a function of modifier concentration. Measurements were performed at room temperature in the microfluidic device at a constant inlet flow rate of 12 mL h^{-1} of growth solution (S = 7.0). RGR values below unity indicate growth inhibition. Each data point represents the average of at least three individual experiments. Error bars span two standard deviations (those not shown are smaller than the symbol). All experiments use conditions where molecules were predominantly deprotonated: pH 7 for alginate and citrate[65, 66], and pH 9 for DTPA.[52] Dashed lines are interpolated to guide the eye.

Barite crystal growth is completely inhibited under low-Re (Re = 9.2) flow in the presence of 0.2 μg mL^{-1} alginate, which is similar to the results obtained under quiescent conditions (Figure 2) at higher alginate concentrations (Figure 5). This result highlights the potency of alginate in comparison with DTPA and citrate, which do not exceed 60% inhibition (where percent inhibition is defined as (1 – RGR) × 100%). The inhibition profiles for DTPA and citrate are similar, although the latter is slightly more effective at suppressing growth along the length of the crystal (Figure 5a). DTPA and citrate are similarly effective at inhibiting barite growth along the width of

crystals (Figure 5b). These observations indicate that DTPA has a minor preference for binding to barite (100) surfaces at lower concentrations (< 0.6 μg mL^{-1}), whereas citrate exhibits non-preferential interactions between (100) and (010) surfaces.

Prior studies of barite crystal growth inhibitors have predominantly assessed their impact on the kinetics of crystallization without examining specific influences on the physical properties of crystals (e.g. size and morphology).[11, 23, 24, 60, 61, 67-69] Here, we use *in situ* optical microscopy to track temporal changes in crystal morphology of barite seed crystals in microfluidic channels under the flow of supersaturated solutions containing alginate (Figures 6a and S8). Time-resolved images reveal that seed crystals grow disproportionately at the apical tips (i.e. {210} facets) and a fraction of crystals exhibit orientation-dependent anisotropic growth. These effects are observed for a minor population of crystals (labelled as "crystals affected by flow"). The asymmetric geometry developed after exposure to growth solutions containing alginate (indicated by white arrows in Figures 6a and S8), leading to crystals with aspect ratios that are much smaller than the average value measured in bulk crystallization assays (i.e. a higher percentage of length-to-width ratios $L/W \leq 2$; see Figure S9). Analysis of crystals affected by flow for different alginate concentrations reveals that asymmetric growth inhibition is more pronounced at lower alginate content (<0.05 μg mL^{-1}). Notably, the {210} facets oriented against the direction of flow grow at a slower rate than those on the opposite sides of the crystal, resulting in abnormal morphologies with longer imaging time. The percentage of crystals affected by flow monotonically decreases from 35% to less than 5% with increasing alginate concentration (Figure 6b). These features are consistent with faster transport of alginate to facets directly facing oncoming solution flow. Previous literature has shown that laminar streams that encounter immobile crystals can generate different secondary flows depending on the crystal orientation.[70] Specifically, these secondary flows produce wakes

near the trailing facets where solute transport to the crystal is reduced. These changes in flow surrounding the crystals can result in morphological instabilities, macrostep formation, and liquid inclusion.

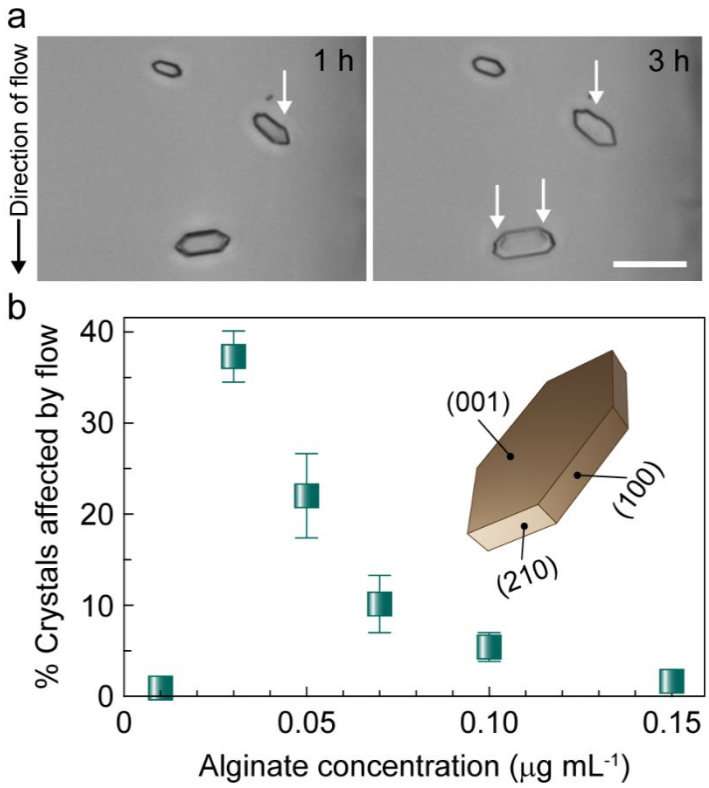

Figure 6. (a) Optical micrographs extracted from Movie S1 after 1 and 3 h of continuous imaging show asymmetric inhibition of barite {210} facets (indicated by white arrows) oriented against the flow of solution. Images show a section of the microchannel where crystal growth is monitored at 21 °C under constant flow (12 mL h^{-1}) of supersaturated growth (S = 7.0) solution containing 0.03 μg mL^{-1} alginate. Scale bar equals 20 μm. (b) Percentage of the crystal population in microchannels that demonstrate asymmetric growth as a function of alginate concentration. Data are the averages from a minimum of 3 separate experiments (at least 50 crystals per experiment). Error bars span two standard deviations. Inset: indexed barite crystal.

Mechanism of Barite Growth Inhibition

Prior studies have used *in situ* AFM to show that barite surfaces grow classically (i.e. layer-by-layer).[71-75] This technique has also been used to examine conditions of barite surface dissolution[75-77] and with respect to the impact of select inhibitors on surface topography (e.g. layer

morphology).[14, 78] To the best of our knowledge, AFM has not been used to elucidate the mechanism(s) of barite growth inhibition in the presence of carboxylate based modifiers. Here, we visualize the growth of barite (001) surfaces at near molecular level using *in situ* AFM to elucidate the mode of action by which alginate fully suppresses layer advancement. At low supersaturation (S = 4.4) barite growth is primarily governed by the formation of rhombohedral growth hillocks that emanate from screw dislocations (Figure 7a and Movie S2). In the presence of alginate, step velocities were measured and compared against step velocities in a pure growth solution. Step advancement is suppressed (Figure S10) with increasing inhibitor concentration (Figure 7b) via a step pinning mechanism (see Figure S11).[79, 80] The morphology of the growth hillock, however, remains largely unchanged after exposure to alginate. Barite growth at slightly higher supersaturation (S = 5.3) occurs by the birth and spread of 2-dimensional (2D) islands with a triangular morphology bound by the [120] and [010] directions (Figure 7c). These 2D nuclei have an average height of 3.6 Å (Figure 7d), which is equal to one-half the barite unit cell dimension (*c*/2). There is a 180-degree inversion of 2D island orientation with each new layer (Figure S12) owing to the 2_1 axis symmetry of barite with alternating sulfate group orientation between each half unit cell.[81-83]

At high alginate concentration (≥ 1 μg mL^{-1}), we observe complete suppression of layer advancement (Figure S13). At lower alginate concentration (e.g. 0.05 μg mL^{-1}), however, we observe bimodal behavior: One fraction of step edges advance at slower rates compared to layer growth in the control, whereas a second fraction of step edges at random orientations are fully suppressed (as indicated by the solid yellow lines in Figure 7e). Sequential images from Movie S3 show that islands growing on the upper terrace of immobilized layers advance until reaching the step edge where growth ceases, leading to the onset of step bunching. This finding is consistent

with scanning electron micrographs (Figure S3) showing the presence of macrosteps on different surfaces of barite crystals obtained from bulk assays at quiescent conditions. Collectively, these results demonstrate a disconnect in modifier efficacy determined by microfluidic assays compared to *in situ* AFM studies.

Alginate demonstrates a greater inhibition potency in macroscopic (microfluidic) studies compared to molecular level studies (*in situ* AFM). Complete barite growth inhibition is observed at alginate concentrations > 0.2 μg mL^{-1} in microfluidic assays, while *in situ* AFM studies require modifier concentrations of 1.5 μg mL^{-1} or greater to achieve the same result. This discrepancy is attributed to the significant differences in fluid cell geometry, which influences flow patterns and mass transport, between rectangular microchannels in the microfluidic device and the AFM fluid cell. Simple geometries such as rectangular microchannels allow for controlled laminar and axial flow at the flow rate investigated (Re = 9.2, 12 mL h^{-1}), whereas the AFM fluid cell design generates a thin film of liquid with a primarily radial flow pattern owing to the perpendicular inlet and outlet relative to the sample. The radial flow pattern combined with the interference of the cantilever probe in AFM studies poses a challenge in accurately mimicking macroscopic flow conditions, which results in mass transport limitations in the growth inhibition studies particularly with bulky modifiers such as alginate.[84]

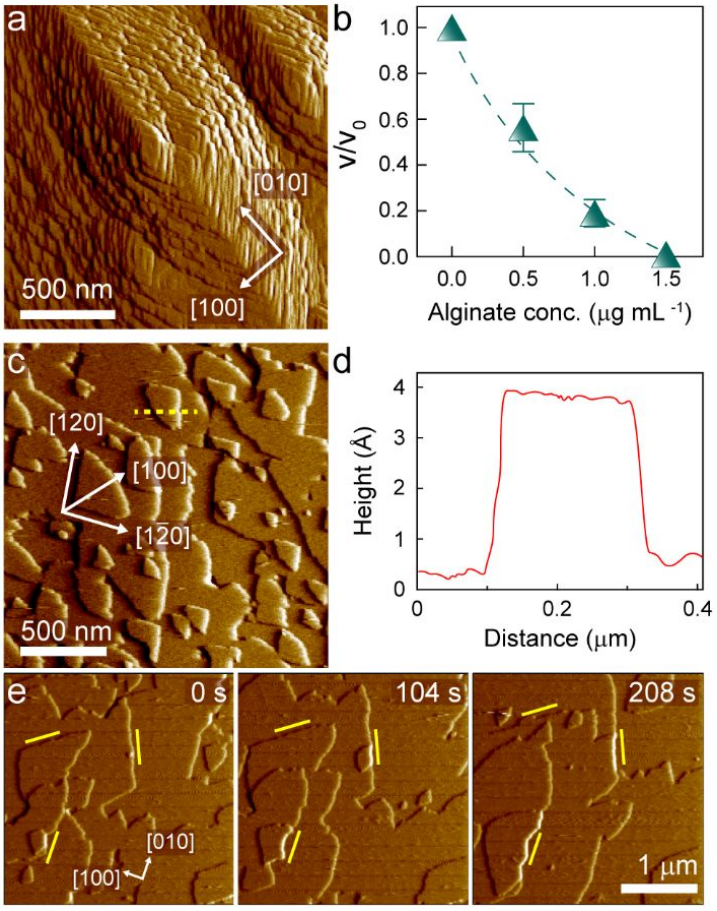

Figure 7. Time-resolved AFM analysis of barite (001) surface growth. (a) Deflection mode image showing spiral growth from a screw dislocation under the flow of growth solution (S = 4.4) containing 1 μg mL^{-1} alginate. (b) Step velocity in the ⟨120⟩ direction for growth solutions containing alginate relative to those without any additive (control) as a function of increasing alginate concentration. Data points are the average of at least 3 separate experiments. Error bars span two standard deviations and the dashed line is interpolated to guide the eye. (c) Representative image of newly formed 2D layers under flow of growth solution at higher supersaturation (S = 5.3). Barite (001) layers exhibit characteristic geometric features with (d) a representative height profile (measured along the dashed yellow line in panel c) indicating single layers with step height h = 3.6 Å. (e) Snapshots from Movie S3 of 2D layer nucleation and advancement in a growth solution (S = 5.3, flow rate = 12 mL h^{-1}) containing 0.05 μg mL^{-1} alginate. Solid yellow lines indicate step edges that are arrested and become sites for the generation of step bunches.

CONCLUSIONS

In this article, we systematically evaluated diverse carboxylate-based molecules as inhibitors of barite crystallization under quiescent and flow conditions. A combination of microfluidics and atomic force microscopy was used to assess growth inhibition from the molecular to macroscopic scale. These findings demonstrated that alginate outperforms other crystal growth modifiers, including common commercial scale treatments such as EDTA and DTPA. One of the unique observations is the full suppression of both nucleation and growth of barite crystals at relatively low alginate concentration (i.e. 0.2 μg mL^{-1}). The superior performance of alginate relative to other carboxylate-based compounds lies in its ability to interact with all principal surfaces of barite crystals. Time-resolved imaging of (001) surface growth during *in situ* AFM measurements reveals that alginate inhibits the advancement of layers via a step pinning mechanism at relatively low supersaturation (S = 4.4). At higher supersaturation (S = 5.3), we observe a transition in the dominant mechanism of inhibition to a step bunching mechanism, which is consistent with macro-step formation observed in bulk assays.

In addition to its dual role as an inhibitor of barite nucleation and crystal growth, there may be practical advantages for replacing current commercial scale inhibitors with alginate. The smaller acid dissociation constants of carboxylate moieties in alginate (pK_{al} = 3.38)[65] relative to more widely used analogues (e.g. DTPA, pK_{av} = 10.5)[85] allow for alginate to be used at neutral pH, thus avoiding caustic chemicals (i.e. metal hydroxides) required in many commercial scale treatments. Moreover, the fact that alginate is readily available in nature and is biodegradable makes it an environmentally friendly alternative to products currently used to suppress the formation of barite scale. Use in practical settings requires further studies to assess the effects of real-world

environmental conditions, particularly temperature and higher solute concentration, on alginate's efficacy as a dual inhibitor of barite nucleation and growth.

Conflicts of interest

There are no conflicts to declare.

Supporting Information. The supporting information is available free of charge at https://pubs.acs.org/doi/10.1021/xxxxxxx. Optical and electron micrographs of crystals from bulk assays; ionic conductivity measurements; barium ion concentration measurements in supernatant solutions at different alginate concentration; powder XRD patterns of crystalline products; time-resolved optical micrographs of crystals during microfluidic assays; statistical analysis of crystal aspect ratios at different alginate concentration; additional AFM images during *in situ* measurements in the presence of alginate; AFM step velocity measurements and data analysis; detailed descriptions of Movies S1 – S3 (PDF).

Acknowledgments. We acknowledge financial support from Shell Oil Company and the National Science Foundation Graduate Student Fellowship (Award DGE 1144207). JDR and JCC also acknowledge support from the Welch Foundation (Awards E-1794 and E-1869, respectively).

REFERENCES

1. Mike Crabtree, D.E., Phil Fletcher, Matt Miller, Ashley Johnson, King George, *Fighting Scale - Removal and Prevention.* Oilfield Review, 1999: 30-45.
2. Hanor, J.S., *Barite–Celestine Geochemistry and Environments of Formation.* Reviews in Mineralogy and Geochemistry, 2000. **40**: 193-275.
3. Li, J., M. Tang, Z. Ye, L. Chen, and Y. Zhou, *Scale formation and control in oil and gas fields: A review.* Journal of Dispersion Science and Technology, 2017. **38**: 661-670.
4. Reynolds, M.A., *A Technical Playbook for Chemicals and Additives Used in the Hydraulic Fracturing of Shales.* Energy & Fuels, 2020.

5. Torres, L., O.P. Yadav, and E. Khan, *Risk assessment of human exposure to Ra-226 in oil produced water from the Bakken Shale.* Science of The Total Environment, 2018. **626**: 867-874.
6. Baynton, A., M.I. Ogden, C.L. Raston, and F. Jones, *Barium sulfate crystallization dependence on upper rim calix [4] arene functional groups.* CrystEngComm, 2012. **14**: 1057-1062.
7. Black, S.N., L.A. Bromley, D. Cottier, R.J. Davey, B. Dobbs, and J.E. Rout, *Interactions at the organic/inorganic interface: binding motifs for phosphonates at the surface of barite crystals.* Journal of the Chemical Society, Faraday Transactions, 1991. **87**: 3409-3414.
8. Coveney, P.V., R. Davey, J.L. Griffin, Y. He, J.D. Hamlin, S. Stackhouse, and A. Whiting, *A new design strategy for molecular recognition in heterogeneous systems: a universal crystal-face growth inhibitor for barium sulfate.* Journal of the American Chemical Society, 2000. **122**: 11557-11558.
9. Jones, F., A. Oliveira, A. Rohl, G. Parkinson, M. Ogden, and M. Reyhani, *Investigation into the effect of phosphonate inhibitors on barium sulfate precipitation.* Journal of Crystal Growth, 2002. **237**: 424-429.
10. Pina, C., C.V. Putnis, U. Becker, S. Biswas, E. Carroll, D. Bosbach, and A. Putnis, *An atomic force microscopy and molecular simulations study of the inhibition of barite growth by phosphonates.* Surface Science, 2004. **553**: 61-74.
11. Bukuaghangin, O., A. Neville, and T. Charpentier. *Scale Formation in Multiphase Conditions*. in *Proceedings of the Oil Field Chemistry Symposium, Gielo*. 2015.
12. Freeman, S.R., F. Jones, M.I. Ogden, A. Oliviera, and W.R. Richmond, *Effect of benzoic acids on barite and calcite precipitation.* Crystal Growth & Design, 2006. **6**: 2579-2587.
13. Jones, F., P. Jones, R. De Marco, B. Pejcic, and A.L. Rohl, *Understanding barium sulfate precipitation onto stainless steel.* Applied Surface Science, 2008. **254**: 3459-3468.
14. Mavredaki, E., A. Neville, and K.S. Sorbie, *Initial stages of barium sulfate formation at surfaces in the presence of inhibitors.* Crystal Growth & Design, 2011. **11**: 4751-4758.
15. Uchida, M., A. Sue, T. Yoshioka, and A. Okuwaki, *Morphology of barium sulfate synthesized with barium (II)–aminocarboxylate chelating precursors.* CrystEngComm, 2001. **3**: 21-26.
16. Nowack, B. and A.T. Stone, *Degradation of Nitrilotris(methylenephosphonic Acid) and Related (Amino)Phosphonate Chelating Agents in the Presence of Manganese and Molecular Oxygen.* Environmental Science & Technology, 2000. **34**: 4759-4765.
17. Means, J.L., T. Kucak, and D.A. Crerar, *Relative degradation rates of NTA, EDTA and DTPA and environmental implications.* Environmental Pollution Series B, Chemical and Physical, 1980. **1**: 45-60.
18. Li, M., H. Cölfen, and S. Mann, *Morphological control of BaSO 4 microstructures by double hydrophilic block copolymer mixtures.* Journal of Materials Chemistry, 2004. **14**: 2269-2276.
19. Qi, L., H. Cölfen, and M. Antonietti, *Control of barite morphology by double-hydrophilic block copolymers.* Chemistry of Materials, 2000. **12**: 2392-2403.
20. Qi, L., H. Cölfen, M. Antonietti, M. Li, J.D. Hopwood, A.J. Ashley, and S. Mann, *Formation of BaSO4 fibres with morphological complexity in aqueous polymer solutions.* Chemistry–A European Journal, 2001. **7**: 3526-3532.
21. Yu, S.-H., M. Antonietti, H. Cölfen, and J. Hartmann, *Growth and self-assembly of BaCrO4 and BaSO4 nanofibers toward hierarchical and repetitive superstructures by polymer-controlled mineralization reactions.* Nano Letters, 2003. **3**: 379-382.
22. Shaw, S.S., K. Sorbie, and L.S. Boak, *The effects of barium sulfate saturation ratio, calcium, and magnesium on the inhibition efficiency: Part II polymeric scale inhibitors.* SPE Production & Operations, 2012. **27**: 390-403.

23. Yan, C., A.T. Kan, F. Zhang, Y. Liu, R.C. Tomson, and M.B. Tomson, *Systematic study of barite nucleation and inhibition with various polymeric scale inhibitors by novel laser apparatus.* SPE Journal, 2015. **20**: 642-651.
24. Leung, W.H. and G.H. Nancollas, *A kinetic study of the seeded growth of barium sulfate in the presence of additives.* Journal of Inorganic and Nuclear Chemistry, 1978. **40**: 1871-1875.
25. Akın, B., M. Öner, Y. Bayram, and K.D. Demadis, *Effects of Carboxylate-Modified, "Green" Inulin Biopolymers on the Crystal Growth of Calcium Oxalate.* Crystal Growth & Design, 2008. **8**: 1997-2005.
26. Boels, L. and G.-J. Witkamp, *Carboxymethyl Inulin Biopolymers: A Green Alternative for Phosphonate Calcium Carbonate Growth Inhibitors.* Crystal Growth & Design, 2011. **11**: 4155-4165.
27. Zhang, H.-p., X.-g. Luo, X.-y. Lin, P.-p. Tang, X. Lu, M.-j. Yang, and Y. Tang, *Biodegradable carboxymethyl inulin as a scale inhibitor for calcite crystal growth: Molecular level understanding.* Desalination, 2016. **381**: 1-7.
28. Ching, S.H., N. Bansal, and B. Bhandari, *Alginate gel particles–A review of production techniques and physical properties.* Critical Reviews in Food Science and Nutrition, 2017. **57**: 1133-1152.
29. Onsøyen, E., *Alginates*, in *Thickening and gelling agents for food*. 1997, Springer. p. 22-44.
30. Tam, S., S. Bilodeau, J. Dusseault, G. Langlois, J.-P. Hallé, and L. Yahia, *Biocompatibility and physicochemical characteristics of alginate–polycation microcapsules.* Acta Biomaterialia, 2011. **7**: 1683-1692.
31. Charlesworth, M., C.J. Kalli, D.G. Thomas, W. Shi, B.F. Graham, Z.M. Aman, and E.F. May, *Compositions and methods for scale inhibition*. 2016, Chevron U.S.A. Inc.
32. Malkaj, P., E. Pierri, and E. Dalas, *The crystallization of hydroxyapatite in the presence of sodium alginate.* Journal of Materials Science: Materials in Medicine, 2005. **16**: 733-737.
33. Nielsen, J.W., K.K. Sand, C.S. Pedersen, L. Lakshtanov, J.R. Winther, M. Willemoës, and S.L.S. Stipp, *Polysaccharide effects on calcite growth: the influence of composition and branching.* Crystal Growth & Design, 2012. **12**: 4906-4910.
34. Olderøy, M.Ø., M. Xie, B.L. Strand, E.M. Flaten, P. Sikorski, and J.-P. Andreassen, *Growth and nucleation of calcium carbonate vaterite crystals in presence of alginate.* Crystal Growth & Design, 2009. **9**: 5176-5183.
35. Wei, L., T. Hong, H. Liu, and T. Chen, *The effect of sodium alginate on struvite crystallization in aqueous solution: a kinetics study.* Journal of Crystal Growth, 2017. **473**: 60-65.
36. Lakshtanov, L., N. Bovet, and S.L.S. Stipp, *Inhibition of calcite growth by alginate.* Geochimica et Cosmochimica Acta, 2011. **75**: 3945-3955.
37. Manoli, F. and E. Dalas, *The effect of sodium alginate on the crystal growth of calcium carbonate.* Journal of Materials Science: Materials in Medicine, 2002. **13**: 155-158.
38. Ucar, S., S.H. Bjørnøy, D.C. Bassett, B.L. Strand, P. Sikorski, and J.-P. Andreassen, *Formation of Hydroxyapatite via Transformation of Amorphous Calcium Phosphate in the Presence of Alginate Additives.* Crystal Growth & Design, 2019. **19**: 7077-7087.
39. Ucar, S., S.H. Bjørnøy, D.C. Bassett, B.L. Strand, P. Sikorski, and J.-P. Andreassen, *Nucleation and Growth of Brushite in the Presence of Alginate.* Crystal Growth & Design, 2015. **15**: 5397-5405.
40. Fan, C., A.T. Kan, P. Zhang, and M.B. Tomson, *Barite Nucleation and Inhibition at 0 to 200* C With and Without Thermodynamic Hydrate Inhibitors.* SPE Journal, 2011. **16**: 440-450.
41. He, S., J.E. Oddo, and M.B. Tomson, *The inhibition of gypsum and barite nucleation in NaCl brines at temperatures from 25 to 90 C.* Applied Geochemistry, 1994. **9**: 561-567.

42. Zhang, F., Z. Dai, C. Yan, N. Bhandari, F. Yan, Y. Liu, Z. Zhang, G. Ruan, A.T. Kan, and M.B. Tomson, *Barite-scaling risk and inhibition at high temperature.* SPE Journal, 2017. **22**: 69-79.
43. Kashchiev, D. and G. Van Rosmalen, *Nucleation in solutions revisited.* Crystal Research Technology: Journal of Experimental Industrial Crystallography, 2003. **38**: 555-574.
44. Burton, W.-K., N. Cabrera, and F. Frank, *The growth of crystals and the equilibrium structure of their surfaces.* Philosophical Transactions of the Royal Society of London. Series A, Mathematical Physical Sciences, 1951. **243**: 299-358.
45. Ma, W., J.F. Lutsko, J.D. Rimer, and P.G. Vekilov, *Antagonistic cooperativity between crystal growth modifiers.* Nature, 2020. **577**: 497-501.
46. Chernov, A.A., *Growth Mechanisms*, in *Modern crystallography III*. 1984, Springer. p. 104-158.
47. Olafson, K.N., T.Q. Nguyen, J.D. Rimer, and P.G. Vekilov, *Antimalarials inhibit hematin crystallization by unique drug–surface site interactions.* Proceedings of the National Academy of Sciences, 2017. **114**: 7531-7536.
48. Olafson, K.N., M.A. Ketchum, J.D. Rimer, and P.G. Vekilov, *Mechanisms of hematin crystallization and inhibition by the antimalarial drug chloroquine.* Proceedings of the National Academy of Sciences, 2015. **112**: 4946-4951.
49. Farmanesh, S., S. Ramamoorthy, J. Chung, J.R. Asplin, P. Karande, and J.D. Rimer, *Specificity of growth inhibitors and their cooperative effects in calcium oxalate monohydrate crystallization.* Journal of the American Chemical Society, 2014. **136**: 367-376.
50. Kim, D., J. Moore, C.P. McCoy, N.J. Irwin, and J.D. Rimer, *Engaging a Battle on Two Fronts: Dual Role of Polyphosphates as Potent Inhibitors of Struvite Nucleation and Crystal Growth.* Chemistry of Materials, 2020. **32**: 8672-8682.
51. Kim, D., C. Olympiou, C.P. McCoy, N.J. Irwin, and J.D. Rimer, *Time-Resolved Dynamics of Struvite Crystallization: Insights from the Macroscopic to Molecular Scale.* Chemistry-A European Journal, 2020. **26**: 3555-3563.
52. Sosa, R.D., X. Geng, M.A. Reynolds, J.D. Rimer, and J.C. Conrad, *A microfluidic approach for probing hydrodynamic effects in barite scale formation.* Lab on a Chip, 2019. **19**: 1534-1544.
53. Yan, F., Z. Dai, G. Ruan, H. Alsaiari, N. Bhandari, F. Zhang, Y. Liu, Z. Zhang, A. Kan, and M. Tomson, *Barite scale formation and inhibition in laminar and turbulent flow: A rotating cylinder approach.* Journal of Petroleum Science Engineering, 2017. **149**: 183-192.
54. Choudhary, M.K., M. Kumar, and J.D. Rimer, *Regulating Nonclassical Pathways of Silicalite-1 Crystallization through Controlled Evolution of Amorphous Precursors.* Angewandte Chemie, 2019. **131**: 15859-15863.
55. Cho, K.R., Y.-Y. Kim, P. Yang, W. Cai, H. Pan, A.N. Kulak, J.L. Lau, P. Kulshreshtha, S.P. Armes, and F.C. Meldrum, *Direct observation of mineral–organic composite formation reveals occlusion mechanism.* Nature Communications, 2016. **7**: 1-7.
56. Lupulescu, A.I. and J.D. Rimer, *In situ imaging of silicalite-1 surface growth reveals the mechanism of crystallization.* Science, 2014. **344**: 729-732.
57. Ma, X., S. Zhang, F. Jiao, C.J. Newcomb, Y. Zhang, A. Prakash, Z. Liao, M.D. Baer, C.J. Mundy, and J. Pfaendtner, *Tuning crystallization pathways through sequence engineering of biomimetic polymers.* Nature Materials, 2017. **16**: 767-774.
58. Nancollas, G.H. and N. Purdie, *Crystallization of barium sulphate in aqueous solution.* Transactions of the Faraday Society, 1963. **59**: 735-740.
59. Blount, C.W., *Synthesis of Barite, Celestite, Anglesite, Witherite, and Strontianite from Aqueous Solutions.* American Mineralogist, 1974. **59**: 1209-1219.

60. Liu, S.T., G.H. Nancollas, and E.A. Gasiecki, *Scanning electron microscopic and kinetic studies of the crystallization and dissolution of barium sulfate crystals.* Journal of Crystal Growth, 1976. **33**: 11-20.
61. Gardner, G.L. and G.H. Nancollas, *Crystal growth in aqueous solution at elevated temperatures. Barium sulfate growth kinetics.* The Journal of Physical Chemistry, 1983. **87**: 4699-4703.
62. Godinho, J.R.A. and A.G. Stack, *Growth Kinetics and Morphology of Barite Crystals Derived from Face-Specific Growth Rates.* Crystal Growth & Design, 2015. **15**: 2064-2071.
63. Gates-Rector, S. and T. Blanton, *The Powder Diffraction File: a quality materials characterization database.* Powder Diffraction, 2019. **34**: 352-360.
64. Blount, C.W., *Barite solubilities and thermodynamic quantities up to 300 C and 1400 bars.* American Mineralogist, 1977. **62**: 942-957.
65. Chuang, J.-J., Y.-Y. Huang, S.-H. Lo, T.-F. Hsu, W.-Y. Huang, S.-L. Huang, and Y.-S. Lin, *Effects of pH on the shape of alginate particles and its release behavior.* International Journal of Polymer Science, 2017. **2017**: Article ID 3902704.
66. Chung, J., R. Sosa, and J.D. Rimer, *Elucidating the Effects of Polyprotic Acid Speciation in Calcium Oxalate Crystallization.* Crystal Growth & Design, 2017. **17**: 4280-4288.
67. Abd-El-Khalek, D., B. Abd-El-Nabey, M.A. Abdel-kawi, S. Ebrahim, and S. Ramadan, *The inhibition of crystal growth of gypsum and barite scales in industrial water systems using green antiscalant.* Water Supply, 2019. **19**: 2140-2146.
68. BinMerdhah, A.B., A.A.M. Yassin, and M.A. Muherei, *Laboratory and prediction of barium sulfate scaling at high-barium formation water.* Journal of Petroleum Science Engineering, 2010. **70**: 79-88.
69. Mady, M.F., P. Bayat, and M.A. Kelland, *Environmentally-Friendly Phosphonated Polyetheramine Scale Inhibitors-Excellent Calcium Compatibility for Oilfield Applications.* Industrial & Engineering Chemistry Research, 2020.
70. Derby, J.J., *Fluid dynamics in crystal growth: The good, the bad, and the ugly.* Progress in Crystal Growth and Characterization of Materials, 2016. **62**: 286-301.
71. Kowacz, M., C.V. Putnis, and A. Putnis, *The effect of cation:anion ratio in solution on the mechanism of barite growth at constant supersaturation: Role of the desolvation process on the growth kinetics.* Geochimica et Cosmochimica Acta, 2007. **71**: 5168-5179.
72. Pina, C., D. Bosbach, M. Prieto, and A. Putnis, *Microtopography of the barite (0 0 1) face during growth:: AFM observations and PBC theory.* Journal of Crystal Growth, 1998. **187**: 119-125.
73. Pina, C.M., U. Becker, P. Risthaus, D. Bosbach, and A. Putnis, *Molecular-scale mechanisms of crystal growth in barite.* Nature, 1998. **395**: 483-486.
74. Pina, C.M., M. Enders, and A. Putnis, *The composition of solid solutions crystallising from aqueous solutions: the influence of supersaturation and growth mechanisms.* Chemical Geology, 2000. **168**: 195-210.
75. Risthaus, P., D. Bosbach, U. Becker, and A. Putnis, *Barite scale formation and dissolution at high ionic strength studied with atomic force microscopy.* Colloids and Surfaces A: Physicochemical and Engineering Aspects, 2001. **191**: 201-214.
76. Kowacz, M., C.V. Putnis, and A. Putnis, *The Control of Solution Composition on Ligand-Promoted Dissolution: DTPA−Barite Interactions.* Crystal Growth & Design, 2009. **9**: 5266-5272.
77. Wang, K.-S., R. Resch, K. Dunn, P. Shuler, Y. Tang, B.E. Koel, and T. Fu Yen, *Dissolution of the barite (001) surface by the chelating agent DTPA as studied with non-contact atomic force microscopy.* Colloids and Surfaces A: Physicochemical and Engineering Aspects, 1999. **160**: 217-227.

78. Pina, C.M., C.V. Putnis, U. Becker, S. Biswas, E.C. Carroll, D. Bosbach, and A. Putnis, *An atomic force microscopy and molecular simulations study of the inhibition of barite growth by phosphonates.* Surface Science, 2004. **553**: 61-74.
79. Cabrera, N., D. Vermilyea, R. Doremus, B. Roberts, and D. Turnbull, *Growth and perfection of crystals.* 1958. **393**.
80. Wang, L., J.J. De Yoreo, X. Guan, S.R. Qiu, J.R. Hoyer, and G.H. Nancollas, *Constant composition studies verify the utility of the Cabrera− Vermilyea (CV) model in explaining mechanisms of calcium oxalate monohydrate crystallization.* Crystal Growth & Design, 2006. **6**: 1769-1775.
81. Bosbach, D., C. Hall, and A. Putnis, *Mineral precipitation and dissolution in aqueous solution: in-situ microscopic observations on barite (001) with atomic force microscopy.* Chemical Geology, 1998. **151**: 143-160.
82. Putnis, A., J.L. Junta-Rosso, and M.F. Hochella, *Dissolution of barite by a chelating ligand: An atomic force microscopy study.* Geochimica et Cosmochimica Acta, 1995. **59**: 4623-4632.
83. Hill, R., *A further refinement of the barite structure.* The Canadian Mineralogist, 1977. **15**: 522-526.
84. Peruffo, M., M.M. Mbogoro, M. Adobes-Vidal, and P.R. Unwin, *Importance of Mass Transport and Spatially Heterogeneous Flux Processes for in Situ Atomic Force Microscopy Measurements of Crystal Growth and Dissolution Kinetics.* The Journal of Physical Chemistry C, 2016. **120**: 12100-12112.
85. Moulin, C., B. Amekraz, V. Steiner, G. Plancque, and E. Ansoborlo, *Speciation Studies on DTPA Using the Complementary Nature of Electrospray Ionization Mass Spectrometry and Time-Resolved Laser-Induced Fluorescence.* Applied Spectroscopy, 2003. **57**: 1151-1161.